

Lateral diffusion induced by active proteins in a biomembrane

Yuto Hosaka, Kento Yasuda, Ryuichi Okamoto, and Shigeyuki Komura*

Department of Chemistry, Graduate School of Science and Engineering, Tokyo Metropolitan University, Tokyo 192-0397, Japan

(Received 14 March 2017; published 16 May 2017)

We discuss the hydrodynamic collective effects due to active protein molecules that are immersed in lipid bilayer membranes and modeled as stochastic force dipoles. We specifically take into account the presence of the bulk solvent that surrounds the two-dimensional fluid membrane. Two membrane geometries are considered: the free membrane case and the confined membrane case. Using the generalized membrane mobility tensors, we estimate the active diffusion coefficient and the drift velocity as a function of the size of a diffusing object. The hydrodynamic screening lengths distinguish the two asymptotic regimes of these quantities. Furthermore, the competition between the thermal and nonthermal contributions in the total diffusion coefficient is characterized by two length scales corresponding to the two membrane geometries. These characteristic lengths describe the crossover between different asymptotic behaviors when they are larger than the hydrodynamic screening lengths.

DOI: [10.1103/PhysRevE.95.052407](https://doi.org/10.1103/PhysRevE.95.052407)**I. INTRODUCTION**

Biomembranes consisting of lipid bilayers can be regarded as thin two-dimensional (2D) fluids, and membrane protein molecules as well as lipid molecules are allowed to move laterally [1,2]. These membrane inclusions are subject to the thermal motion of lipid molecules, leading to random positional fluctuations. Such Brownian motion plays important roles in various life processes, such as the transportation of materials or the reaction between chemical species [3]. To describe lateral diffusion of membrane proteins, a drag coefficient of a cylindrical disk moving in a 2D fluid sheet has been studied theoretically in various membrane environments [4–10]. The obtained drag coefficient was used to estimate the diffusion coefficients of membrane proteins through Einstein’s relation under the assumption that the system is in thermal equilibrium [11].

In recent experiments, however, it has been shown that motions of particles inside cells are dominantly driven by random nonthermal forces rather than thermal fluctuations [12,13]. In these experimental works, they found that nonthermal forces in biological cells are generated by active proteins undergoing conformational changes with a supply of adenosine triphosphate (ATP). These active fluctuations lead to enhanced diffusion of molecules in the cytoplasm [14,15]. Biomembranes also contain various active proteins that act, for example, as ion pumps by changing their shapes to exert forces to the adjacent membrane and solvent [2]. Lipid bilayers containing such active proteins have been called “active membranes,” and their out-of-plane fluctuations (deformations) have already been investigated both experimentally and theoretically [16–18]. However, lateral motions of inclusions in membranes that are induced by active proteins have not yet been considered. Since such active forces give rise to enhanced diffusion, one needs to take into account both active nonthermal fluctuations as well as passive thermal ones to calculate diffusion in membranes.

Recently, Mikhailov and Kapral discussed enhanced diffusion due to nonthermal fluctuating hydrodynamic flows, which are induced by oscillating active force dipoles [see Fig. 1(a)]

[19,20]. They calculated the active diffusion coefficient of a passive particle immersed either in a three-dimensional (3D) cytoplasm or in a 2D membrane, and they showed that it exhibits a logarithmic size dependence for the 2D case. Moreover, a chemotaxis-like drift of a passive particle was predicted when gradients of active proteins or ATP are present [19]. Later, Koyano *et al.* showed that lipid membrane rafts, in which active proteins are concentrated, can induce a directed drift velocity near the interface of a domain [21]. In these works, they considered membranes that are smaller in size than the hydrodynamic screening length. Huang *et al.* performed coarse-grained simulations of active protein inclusions in lipid bilayers [22,23]. In Ref. [23], they showed that active proteins undergoing conformational motions not only affect the membrane shape but also laterally stir the lipid bilayer so that lipid flows are induced. Importantly, the flow pattern induced by an immobilized protein resembles the 2D fluid velocity fields that are created by a force dipole.

Following Refs. [19,20], we assume that an active protein behaves like an oscillating force dipole, which acts on the surroundings to generate hydrodynamic flows that can induce motions of passive particles in the fluid. In this paper, we investigate active diffusion and drift velocity of a particle in “free” and “confined” membranes, which are completely flat and infinitely large. In the free membrane case, a thin 2D fluid sheet is embedded in a 3D solvent having typically a lower viscosity than that of the membrane. In the confined case, which mimics a supported membrane [24], a membrane is sandwiched by two rigid walls separated by a finite but small distance from it. For both the free and confined membrane cases, we employ general mobility tensors that take into account the hydrodynamic effects mediated by the surrounding 3D solvent [25–28]. Using the general mobility tensors, we numerically calculate the active diffusion coefficient and the drift velocity as a function of the diffusing particle size for the entire length scales. Furthermore, several asymptotic expressions are also derived in order to compare with numerical estimates and thermal contributions. Importantly, our result leads to characteristic length scales describing a crossover from nonthermal to thermal diffusive behaviors for large scales.

In the next section, we present the expressions for the active diffusion coefficient and the drift velocity in 2D membranes

*komura@tmu.ac.jp

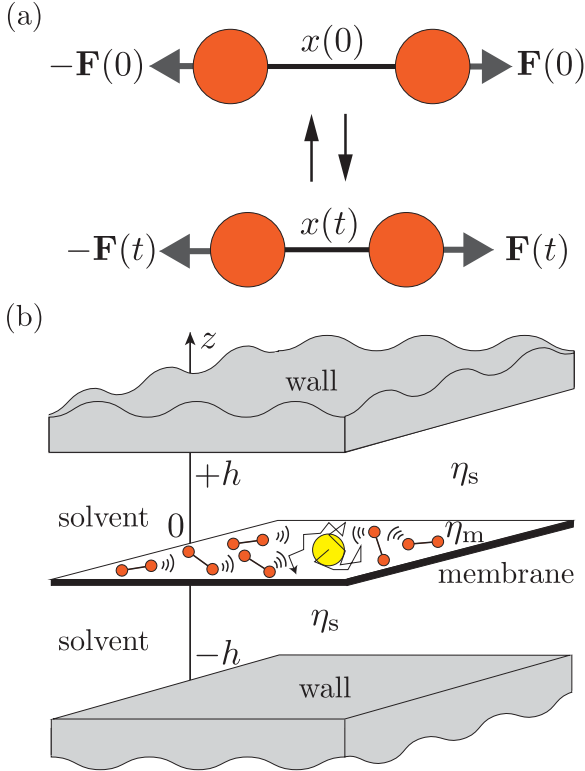


FIG. 1. (a) The conformational change of an oscillating force dipole representing an active protein. Within a turnover cycle of the force dipole separated by a distance $x(t)$, it exerts two oppositely directed forces $\pm \mathbf{F}(t)$ at time t . The integral intensity of a force dipole is S (see the text). (b) Schematic picture showing a flat and infinitely large membrane of 2D viscosity η_m that is located at $z = 0$. The membrane is surrounded by a bulk solvent of 3D viscosity η_s , and the two flat walls are located at $z = \pm h$. The solvent velocity is assumed to vanish at the surfaces of these walls. The “free membrane” and the “confined membrane” cases correspond to the limits of $h \rightarrow \infty$ and $h \rightarrow 0$, respectively. The yellow passive particle undergoes Brownian motion due to thermal and nonthermal fluctuations. The latter contribution is induced by active force dipoles that are distributed homogeneously in the membrane with a 2D concentration c_0 .

[19]. We also review the general mobility tensors for the free and confined membrane cases [25–28]. Using these expressions, we calculate in Sec. III the active diffusion coefficient for the two geometries. In Sec. IV, we compare the thermal diffusion coefficient with the obtained nonthermal diffusion coefficient, and we discuss the characteristic crossover lengths. In Sec. V, we obtain the drift velocities as a function of the particle size. A summary of our work and some numerical estimates for the obtained quantities are given in Sec. VI.

II. ACTIVE TRANSPORT AND MOBILITY TENSORS IN MEMBRANES

A. Active diffusion coefficient

Active proteins in a 2D biological membrane, modeled as oscillating force dipoles, produce nonequilibrium fluctuations and cause an enhancement of the lateral diffusion of a passive particle. We assume that the spatially fixed force dipoles are

homogeneously and isotropically distributed in the membrane, and they exert only in-plane lateral forces. The total diffusion coefficient is given by $D = D_T + D_A$, where D_T is the thermal contribution and is determined by Einstein’s relation (which will be discussed in Sec. IV), and D_A is the active nonthermal contribution given by [19]

$$D_A = \frac{Sc_0}{2} \int d^2r \Omega_{\beta\beta'\gamma\gamma'} \frac{\partial G_{\alpha\beta}(\mathbf{r})}{\partial r_\gamma} \frac{\partial G_{\alpha\beta'}(\mathbf{r})}{\partial r_{\gamma'}}, \quad (1)$$

where $\mathbf{r} = (x, y)$ denotes a 2D vector and we have introduced a notation

$$\Omega_{\beta\beta'\gamma\gamma'} = \frac{1}{8}(\delta_{\beta\beta'}\delta_{\gamma\gamma'} + \delta_{\beta\gamma}\delta_{\beta'\gamma'} + \delta_{\beta\gamma'}\delta_{\beta'\gamma}). \quad (2)$$

Throughout this paper, the summation over repeated greek indices is assumed. In Eq. (1), S is the integral intensity of a force dipole, c_0 is the constant 2D concentration of active proteins, and $G_{\alpha\beta}(\mathbf{r})$ is the membrane mobility tensor, which will be discussed later separately.

Within a fluctuating “dimer model” as presented in Fig. 1(a), the magnitude of a force dipole is given by $m(t) = x(t)F(t)$, where $x(t)$ is the distance between the two spheres and $F(t)$ is the magnitude of the oppositely directed forces. The statistical average of the dipole magnitude vanishes, i.e., $\langle m(t) \rangle = 0$, whereas the integral intensity S of a force dipole is given by $S = \int_0^\infty dt \langle m(t)m(0) \rangle$ [19]. Since we assume that active proteins are homogeneously distributed in the membrane as shown in Fig. 1(b), it is sufficient to consider only the isotropic diffusion as given by Eq. (1).

In deriving Eq. (1), the size of a dipole is assumed to be much smaller than the distance between the passive particle and active force dipoles [19]. At large distances, almost any object that changes its shape would create a flow field that corresponds to some force dipole. It should be noted, however, that the above expression is not accurate when the distance between them becomes smaller. As for the mobility tensor in 3D fluids, it is known that the Rotne-Prager mobility tensor takes into account higher-order corrections to the Oseen mobility tensor and gives a more accurate approximation at short distances [20]. Such a better approximation has not been worked out so far for 2D fluid membranes, and we shall only consider the lowest-order contribution (see later calculations). In the above, we have also assumed that force dipoles are spatially fixed in the membrane. Since no forces are applied to fix the dipoles, such an approximation is justified when the dynamics of force dipoles is much slower than that of the passive particle.

B. Drift velocity

Although we have assumed above that c_0 is constant, active proteins are often distributed inhomogeneously in the membrane due to heterogeneous structures such as sphingolipid-enriched domains [29,30]. According to the “lipid raft” hypothesis, these domains act as platforms for membrane signaling and trafficking [31]. Hence it is also important to consider the effects of nonuniform spatial distribution of active proteins and to see how it affects the lateral dynamics in membranes.

When a spatial concentration gradient ∇c of active protein is present, it gives rise to an unbalanced induced force between two points in the membrane. Hence passive particles are subjected to a drift toward either lower or higher concentration of active proteins, and a chemotaxis-like drift can occur. When the absolute value of the concentration gradient $|\nabla c|$ is assumed to be constant, the induced drift velocity of a passive particle in the direction ∇c is given by [19]

$$V = -S|\nabla c| \int d^2r \Omega_{\beta\beta'\gamma\gamma'} \hat{n}_\alpha \frac{\partial^2 G_{\alpha\beta}(\mathbf{r})}{\partial r_\gamma \partial r_\delta} \frac{\partial G_{\delta\beta'}(\mathbf{r})}{\partial r_{\gamma'}} (\mathbf{r} \cdot \hat{\mathbf{n}}). \quad (3)$$

Here, the unit vector $\hat{\mathbf{n}} = \nabla c/|\nabla c|$ denotes the direction of the concentration gradient of active proteins. We shall employ the above expression to obtain the lateral drift velocity in a membrane by using the membrane mobility tensor as discussed below.

C. Membrane mobility tensors

Since we discuss active diffusion in an infinitely large flat membrane, we use the 2D membrane mobility tensor, which also takes into account the hydrodynamic effects of the surrounding 3D solvent. We consider a general situation as depicted in Fig. 1(b), where a fluid membrane of 2D shear viscosity η_m is surrounded by a solvent of 3D shear viscosity η_s . Furthermore, we consider the case in which there are two walls located symmetrically at an arbitrary distance h from the flat membrane [25–28].

We denote the in-plane velocity vector of the fluid membrane by $\mathbf{v}(\mathbf{r})$ and the lateral pressure by $p(\mathbf{r})$. Assuming that the incompressibility condition holds for the fluid membrane, we write its hydrodynamic equations as

$$\nabla \cdot \mathbf{v} = 0, \quad (4)$$

$$\eta_m \nabla^2 \mathbf{v} - \nabla p + \mathbf{f}_s + \mathbf{F} = 0. \quad (5)$$

The second equation is the 2D Stokes equation, where \mathbf{f}_s is the force exerted on the membrane by the surrounding solvent, and \mathbf{F} is any external force acting on the membrane. If we denote the upper and lower solvents with the superscripts \pm , the two solvent velocities $\mathbf{v}^\pm(\mathbf{r}, z)$ and pressures $p^\pm(\mathbf{r}, z)$ obey the following hydrodynamic equations, respectively:

$$\hat{\nabla} \cdot \mathbf{v}^\pm = 0, \quad (6)$$

$$\eta_s \hat{\nabla}^2 \mathbf{v}^\pm - \hat{\nabla} p^\pm = 0, \quad (7)$$

where $\hat{\nabla}$ stands for the 3D differential operator.

We assume that the surrounding solvent cannot permeate the membrane, and we impose the no-slip boundary condition between the membrane and the surrounding solvent at $z = 0$ [4,5,25–28]. Hence we require the conditions

$$v_z^\pm(\mathbf{r}, 0) = 0, \quad v_\alpha(\mathbf{r}) = v_\alpha^\pm(\mathbf{r}, 0), \quad (8)$$

where $\alpha = x, y$. Furthermore, the solvent velocity vanishes at the walls located at $z = \pm h$, i.e., $v_\alpha^\pm(\mathbf{r}, \pm h) = 0$.

By solving the above coupled hydrodynamic equations in Fourier space with $\mathbf{k} = (k_x, k_y)$ being the 2D wave vector, the 2D mobility tensor $G_{\alpha\beta}(\mathbf{k})$ defined through $v_\alpha(\mathbf{k}) =$

$G_{\alpha\beta}(\mathbf{k}) F_\beta(\mathbf{k})$ can be obtained as [25–28]

$$G_{\alpha\beta}(\mathbf{k}) = \frac{\delta_{\alpha\beta} - \hat{k}_\alpha \hat{k}_\beta}{\eta_m [k^2 + \nu k \coth(kh)]}, \quad (9)$$

where $k = |\mathbf{k}|$ and $\hat{k}_\alpha = k_\alpha/k$, and the ratio of the two viscosities $\nu^{-1} = \eta_m/(2\eta_s)$ defines the Saffman-Delbrück (SD) hydrodynamic screening length [4,5]. Notice that η_m and η_s have different dimensions, and ν^{-1} has a dimension of length.

To perform analytical calculations, the two limiting cases of Eq. (9) are considered, i.e., the “free membrane” case and the “confined membrane” case corresponding to the limits of $h \rightarrow \infty$ and $h \rightarrow 0$, respectively [26–28]. For the free membrane case, we take the limit $kh \gg 1$ in Eq. (9) and obtain the following asymptotic expression:

$$G_{\alpha\beta}^F(\mathbf{k}) = \frac{\delta_{\alpha\beta} - \hat{k}_\alpha \hat{k}_\beta}{\eta_m (k^2 + \nu k)}. \quad (10)$$

Hereafter, we shall denote the quantities for the free membrane case with the superscript “F.” For the confined membrane case, on the other hand, we take the opposite limit $kh \ll 1$ and obtain

$$G_{\alpha\beta}^C(\mathbf{k}) = \frac{\delta_{\alpha\beta} - \hat{k}_\alpha \hat{k}_\beta}{\eta_m (k^2 + \kappa^2)}, \quad (11)$$

where $\kappa^{-1} = (h/\nu)^{1/2}$ is the Evans-Sackmann (ES) screening length [7], and we use the superscript “C” for the quantities related to the confined membrane case. We note that the ES screening length κ^{-1} is the geometric mean of ν^{-1} and h so that we typically have $\kappa^{-1} < \nu^{-1}$.

Taking the inverse Fourier transform of Eqs. (10) and (11), we obtain the mobility tensors in real space for the two limiting cases as [26–28]

$$G_{\alpha\beta}^F(\mathbf{r}) = \frac{1}{4\eta_m} \left[\mathbf{H}_0(\nu r) - Y_0(\nu r) + \frac{2}{\pi \nu^2 r^2} - \frac{\mathbf{H}_1(\nu r)}{\nu r} + \frac{Y_1(\nu r)}{\nu r} \right] \delta_{\alpha\beta} + \frac{1}{4\eta_m} \left[-\frac{4}{\pi \nu^2 r^2} + \frac{2\mathbf{H}_1(\nu r)}{\nu r} - \frac{2Y_1(\nu r)}{\nu r} - \mathbf{H}_0(\nu r) + Y_0(\nu r) \right] \hat{r}_\alpha \hat{r}_\beta \quad (12)$$

and

$$G_{\alpha\beta}^C(\mathbf{r}) = \frac{1}{2\pi \eta_m} \left[K_0(\kappa r) + \frac{K_1(\kappa r)}{\kappa r} - \frac{1}{\kappa^2 r^2} \right] \delta_{\alpha\beta} + \frac{1}{2\pi \eta_m} \left[-K_0(\kappa r) - \frac{2K_1(\kappa r)}{\kappa r} + \frac{2}{\kappa^2 r^2} \right] \hat{r}_\alpha \hat{r}_\beta, \quad (13)$$

respectively, where we have used the notations $r = |\mathbf{r}|$ and $\hat{r}_\alpha = r_\alpha/r$. In the above, $\mathbf{H}_n(z)$ are the Struve functions, $Y_n(z)$ are the Bessel functions of the second kind, and $K_n(z)$ are the modified Bessel functions of the second kind. The physical meaning of the above expressions was also discussed in Refs. [32–34]. We note that if there is only one wall instead of two, the definition of the ES length needs to be modified as $\kappa^{-1} \rightarrow (2h/\nu)^{1/2}$ [34]. In the next sections, we shall use

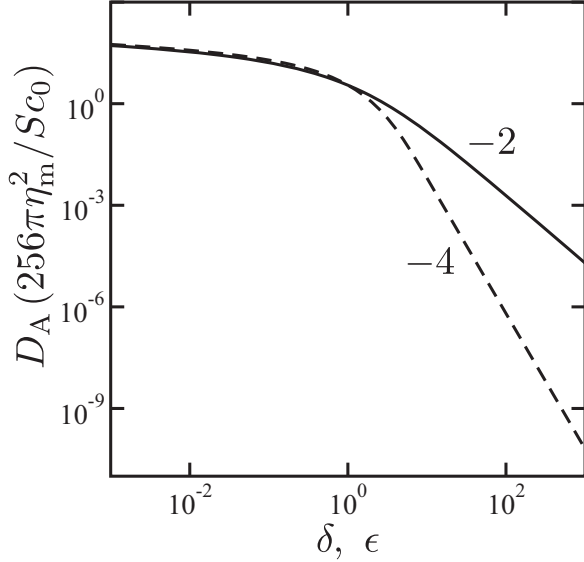


FIG. 2. The plot of the scaled active diffusion coefficient D_A as a function of the scaled cutoff length $\delta = \nu \ell_c$ and $\epsilon = \kappa \ell_c$ for the free membrane case [solid line, see Eq. (14)] and the confined membrane case [dashed line, see Eq. (19)], respectively. Here D_A is scaled by $S c_0 / (256\pi \eta_m^2)$. The numbers in this plot indicate the slope of the curves and represent the powers of the algebraic dependencies.

Eqs. (12) and (13) to calculate the active diffusion coefficients and the drift velocity.

III. ACTIVE DIFFUSION COEFFICIENT

A. Free membranes

We first calculate the active diffusion coefficient for the free membrane case by substituting Eq. (12) into Eq. (1). Since the integrand in Eq. (1) diverges logarithmically at short distances, we need to introduce a small cutoff length ℓ_c . Physically, ℓ_c is given by the sum of the size of a passive particle (undergoing lateral Brownian motion) and that of a force dipole [20]. In the following, we generally assume that force dipoles are smaller than the diffusing object, whose size is represented by ℓ_c . This is further justified when we consider lateral diffusion of a passive object that is larger than the SD or ES screening lengths.

Introducing a dimensionless vector $\mathbf{z} = \nu \mathbf{r}$ scaled by the SD length, we can write the active diffusion coefficient for the free membrane case as

$$D_A^F = \frac{S c_0}{32\pi^2 \eta_m^2} \int_{\delta}^{\infty} d^2 z \Omega_{\beta\beta'\gamma\gamma'} \frac{\partial g_{\alpha\beta}^F(\mathbf{z})}{\partial z_\gamma} \frac{\partial g_{\alpha\beta'}^F(\mathbf{z})}{\partial z_{\gamma'}}, \quad (14)$$

where $\delta = \nu \ell_c$ is the dimensionless cutoff, and $g_{\alpha\beta}^F(\mathbf{z}) = 4\pi \eta_m G_{\alpha\beta}^F$ is the corresponding dimensionless mobility tensor [see Eq. (12)]. We have first evaluated the above integral numerically. In Fig. 2, we plot the obtained D_A^F as a function of $\delta = \nu \ell_c$ by the solid line. We see that the active diffusion coefficient depends only weakly on the particle size at small scales, whereas it shows a stronger size dependence described by a power-law behavior at large scales. The crossover between these two behaviors is set by the condition $\delta \approx 1$.

To understand the above behaviors, we next discuss the asymptotic behaviors of D_A^F for both small and large δ values. Expanding the mobility tensor in Eq. (12) for $\nu r \ll 1$ and $\nu r \gg 1$, we have [34]

$$g_{\alpha\beta}^F(\mathbf{z}) \approx \left(\ln \frac{2}{z} - \gamma - \frac{1}{2} \right) \delta_{\alpha\beta} + \hat{z}_\alpha \hat{z}_\beta \quad (15)$$

and

$$g_{\alpha\beta}^F(\mathbf{z}) \approx \frac{2}{z} \hat{z}_\alpha \hat{z}_\beta, \quad (16)$$

respectively, where $\gamma = 0.5722\dots$ is Euler's constant. By substituting Eqs. (15) and (16) into Eq. (14), we can analytically obtain the asymptotic forms of the active diffusion coefficient as a function of $\delta = \nu \ell_c$.

As obtained in Ref. [19], we find for $\delta \ll 1$

$$D_A^F \approx \frac{S c_0}{32\pi \eta_m^2} \ln \frac{L}{\ell_c}, \quad (17)$$

where a large cutoff length L is introduced because the integral in Eq. (14) also diverges logarithmically at large distances. To match with the numerical estimation, we obtain $L \approx 0.682\nu^{-1}$. The above logarithmic dependence on ℓ_c means that D_A^F depends only weakly on the particle size. We also note that the above expression contains only the membrane viscosity η_m , and does not depend on the solvent viscosity η_s . This is because the hydrodynamics at small scales is primarily dominated by the 2D membrane property.

In the opposite limit of $\delta \gg 1$, on the other hand, we show in Appendix A that the active diffusion coefficient becomes

$$D_A^F \approx \frac{5 S c_0}{256\pi \eta_s^2} \frac{1}{\ell_c^2}, \quad (18)$$

which is an important result of this paper. This asymptotic expression decays as $1/\ell_c^2$ and depends now only on η_s , indicating that the membrane lateral dynamics is governed by the surrounding 3D fluid at large scales. From the obtained asymptotic expressions in Eqs. (17) and (18), the behavior of D_A^F in Fig. 2 is explained as a crossover from a logarithmic dependence to an algebraic dependence with a power of -2 .

B. Confined membranes

Next we consider the confined membrane case. With the use of Eq. (13), the active diffusion coefficient can be written as

$$D_A^C = \frac{S c_0}{32\pi^2 \eta_m^2} \int_{\epsilon}^{\infty} d^2 w \Omega_{\beta\beta'\gamma\gamma'} \frac{\partial g_{\alpha\beta}^C(\mathbf{w})}{\partial w_\gamma} \frac{\partial g_{\alpha\beta'}^C(\mathbf{w})}{\partial w_{\gamma'}}, \quad (19)$$

where $\mathbf{w} = \kappa \mathbf{r}$ is a different dimensionless variable, $\epsilon = \kappa \ell_c$ is a differently scaled cutoff, and $g_{\alpha\beta}^C(\mathbf{w}) = 4\pi \eta_m G_{\alpha\beta}^C$ is the corresponding dimensionless mobility tensor [see Eq. (13)]. Performing the numerical integration of Eq. (19), we plot in Fig. 2 the active diffusion coefficient D_A^C as a function of $\epsilon = \kappa \ell_c$ by the dashed line. For small ϵ values, the behavior of D_A^C is similar to that of D_A^F , while D_A^C decays much faster than D_A^F for large ϵ values.

To discuss these size dependencies, we use the asymptotic expressions of Eq. (13) for $\kappa r \ll 1$ and $\kappa r \gg 1$ given by [34]

$$g_{\alpha\beta}^C(\mathbf{w}) \approx \left(\ln \frac{2}{w} - \gamma - \frac{1}{2} \right) \delta_{\alpha\beta} + \hat{w}_\alpha \hat{w}_\beta \quad (20)$$

and

$$g_{\alpha\beta}^C(\mathbf{w}) \approx -\frac{2}{w^2} (\delta_{\alpha\beta} - 2\hat{w}_\alpha \hat{w}_\beta), \quad (21)$$

respectively. Note that Eq. (20) is identical to Eq. (15) when w is replaced by z . Hence, in the limit of $\epsilon \ll 1$, the active diffusion coefficient for the confined membrane case should be identical to Eq. (17) and is given by [19]

$$D_A^C \approx \frac{Sc_0}{32\pi\eta_m^2} \ln \frac{L}{\ell_c}. \quad (22)$$

The large cutoff length should be taken here as $L \approx 1.12\kappa^{-1}$. As mentioned before, the 2D hydrodynamic effect is more important at small scales, and D_A^C is logarithmically dependent on the particle size.

In the large size limit of $\epsilon \gg 1$, on the other hand, we also show in Appendix A that D_A^C behaves asymptotically as

$$D_A^C \approx \frac{Sc_0}{16\pi\eta_s^2} \frac{h^2}{\ell_c^4}, \quad (23)$$

which is another important result. The obtained expression decays as $1/\ell_c^4$, which is much stronger than Eq. (18) for the free membrane case. According to Eqs. (22) and (23), the behavior of D_A^C in Fig. 2 can be understood as a crossover from a logarithmic dependence to an algebraic dependence with a power of -4 .

IV. TOTAL DIFFUSION COEFFICIENT

Having obtained the active diffusion coefficients for the free and the confined membrane cases, we now discuss the total lateral diffusion coefficients in membranes by considering both thermal and nonthermal contributions. Concerning the thermal diffusion coefficient D_T^F for the free membrane case, we use an empirical expression obtained by Petrov and Schuille [35,36],

$$D_T^F(\delta) = \frac{k_B T}{4\pi\eta_m} \left[\ln \frac{2}{\delta} - \gamma + \frac{4\delta}{\pi} - \frac{\delta^2}{2} \ln \frac{2}{\delta} \right] \times \left[1 - \frac{\delta^3}{\pi} \ln \frac{2}{\delta} + \frac{c_1 \delta^{b_1}}{1 + c_2 \delta^{b_2}} \right]^{-1}, \quad (24)$$

where k_B is the Boltzmann constant, T is the temperature, and the four numerical constants are chosen as $c_1 = 0.73761$, $b_1 = 2.74819$, $c_2 = 0.52119$, and $b_2 = 0.51465$ [36]. For the free membrane case, there is no exact analytical expression of the thermal diffusion coefficient that covers the entire size range, except for the case in which a 2D polymer chain is confined in a fluid membrane [26]. Equation (24) is known to recover the correct asymptotic limits of the thermal diffusion coefficients both for $\delta \ll 1$ [4,5] and $\delta \gg 1$ [6].

On the other hand, the thermal diffusion coefficient D_T^C for the confined membrane case was explicitly calculated by Evans *et al.* [7] and also by Ramachandran *et al.* [8–11]. In

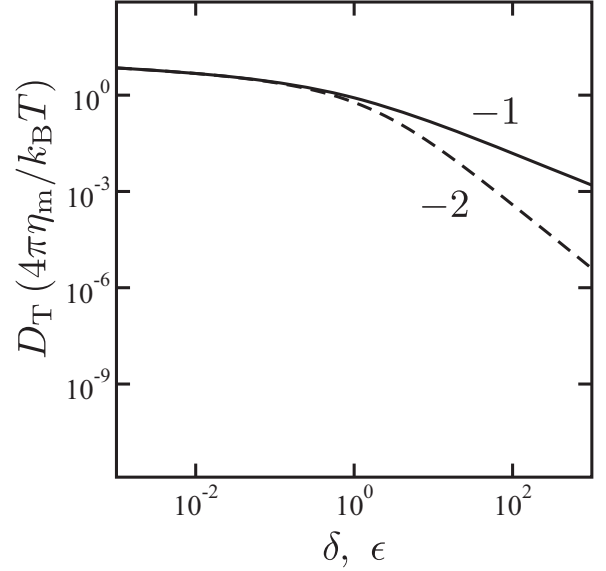


FIG. 3. The plot of the scaled thermal diffusion coefficient D_T as a function of the scaled cutoff length $\delta = \nu\ell_c$ and $\epsilon = \kappa\ell_c$ for the free membrane case [solid line, see Eq. (24)] and the confined membrane case [dashed line, see Eq. (25)], respectively. Here D_T is scaled by $k_B T/(4\pi\eta_m)$. The numbers in this plot indicate the slope of the curves and represent the powers of the algebraic dependencies.

this case, the resulting expression is given by

$$D_T^C(\epsilon) = \frac{k_B T}{4\pi\eta_m} \left[\frac{\epsilon^2}{4} + \frac{\epsilon K_1(\epsilon)}{K_0(\epsilon)} \right]^{-1}. \quad (25)$$

In Fig. 3, we plot D_T^F as a function of the particle size δ by the solid line, and D_T^C as a function of ϵ by the dashed line for the whole size range. Their asymptotic behaviors are discussed separately below.

When we consider the total diffusion coefficient $D = D_T + D_A$, we shall neglect the contribution from thermal fluctuations of force dipoles. These fluctuations can arise when force dipoles contain structural internal degrees of freedom. However, such a contribution to the diffusion coefficient is small compared to D_T because it should be proportional to the product of $k_B T$ and the concentration of force dipoles c_0 .

A. Free membranes

For the free membrane case, the total diffusion coefficient is given by $D^F = D_T^F + D_A^F$, where the active nonthermal contribution D_A^F was discussed in the previous section. Using Eqs. (24) and (17) in the limit of $\delta \ll 1$, we asymptotically have [4,5]

$$D^F \approx \frac{k_B T}{4\pi\eta_m} \left(\ln \frac{2}{\nu\ell_c} - \gamma \right) + \frac{Sc_0}{32\pi\eta_m^2} \ln \frac{L}{\ell_c}, \quad (26)$$

where both contributions are proportional to $\ln(1/\ell_c)$.

For $\delta \gg 1$, on the other hand, we obtain from Eqs. (24) and (18) [6]

$$D^F \approx \frac{k_B T}{16\eta_s} \frac{1}{\ell_c} + \frac{5Sc_0}{256\pi\eta_s^2} \frac{1}{\ell_c^2}. \quad (27)$$

Since the ℓ_c -dependencies in Eq. (27) are different between the thermal and nonthermal contributions, we can introduce a new crossover length defined by

$$\ell^* = \frac{5Sc_0}{16\pi k_B T \eta_s}. \quad (28)$$

This length scale characterizes a crossover from the $1/\ell_c^2$ -dependence to the $1/\ell_c$ -dependence. When $\ell_c \ll \ell^*$ (but still $\nu^{-1} \ll \ell_c$), the nonthermal contribution dominates over the thermal one, while in the opposite limit of $\ell_c \gg \ell^*$ the thermal contribution is of primary importance.

B. Confined membranes

In the case of confined membranes, the total diffusion coefficient now becomes $D^C = D_T^C + D_A^C$. In the limit of $\epsilon \ll 1$, we have from Eqs. (25) and (22) [7,8]

$$D^C \approx \frac{k_B T}{4\pi \eta_m} \left(\ln \frac{2}{\kappa \ell_c} - \gamma \right) + \frac{Sc_0}{32\pi \eta_m^2} \ln \frac{L}{\ell_c}, \quad (29)$$

where both contributions exhibit a logarithmic dependence on ℓ_c as in the free membrane case.

In the opposite limit of $\epsilon \gg 1$, we find from Eqs. (25) and (23) [7,8]

$$D^C \approx \frac{k_B T}{2\pi \eta_s} \frac{h}{\ell_c^2} + \frac{Sc_0}{16\pi \eta_s^2} \frac{h^2}{\ell_c^4}. \quad (30)$$

Similar to the free membrane case, we can consider another characteristic length defined by

$$\ell^{**} = \left(\frac{Sc_0 h}{8k_B T \eta_s} \right)^{1/2}. \quad (31)$$

This length scale characterizes a crossover from the $1/\ell_c^4$ -dependence to the $1/\ell_c^2$ -dependence. We note that ℓ^{**} is essentially the geometric mean of ℓ^* and h . Numerical estimates of these two characteristic length scales will be discussed in Sec. VI.

V. DRIFT VELOCITY

A. Free membranes

In this section, we calculate the drift velocity V of a passive particle due to a concentration gradient of active force dipoles. For the free membrane case, we substitute Eq. (12) into Eq. (3) and obtain

$$V^F = - \frac{S|\nabla c|}{16\pi^2 \eta_m^2} \int_{\delta}^{\infty} d^2 z \Omega_{\beta\beta'\gamma\gamma'} \times \hat{n}_\alpha \frac{\partial^2 g_{\alpha\beta}^F(\mathbf{z})}{\partial z_\gamma \partial z_\delta} \frac{\partial g_{\delta\beta'}^F(\mathbf{z})}{\partial z_{\gamma'}} (\mathbf{z} \cdot \hat{\mathbf{n}}), \quad (32)$$

where $\delta = \nu \ell_c$ and $g_{\alpha\beta}^F(\mathbf{z}) = 4\pi \eta_m G_{\alpha\beta}^F$ as before. Performing the numerical integration of Eq. (32), we plot in Fig. 4 the drift velocity V^F as a function of δ by the solid line. Similar to the active diffusion coefficient D_A^F , the drift velocity V^F depends weakly on the particle size at small scales, while it exhibits a stronger size dependence at large scales. Such a crossover also occurs around $\delta \approx 1$.

We next discuss the asymptotic behaviors of V^F for small and large δ values. With the use of Eqs. (15) and (16), we show

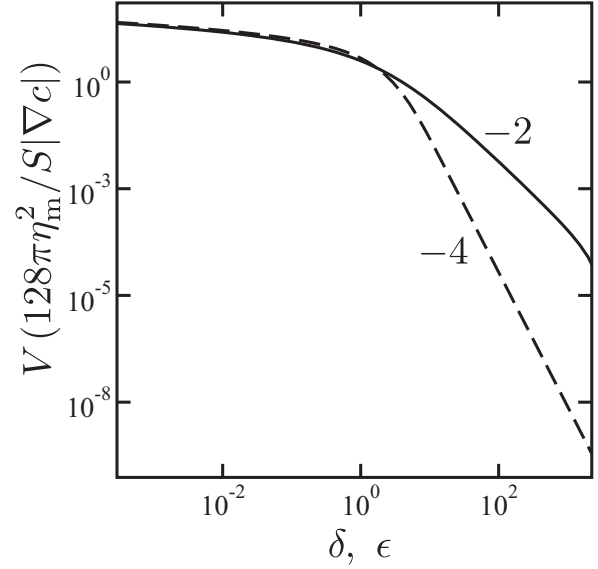


FIG. 4. The plot of the scaled drift velocity V as a function of the scaled cutoff length $\delta = \nu \ell_c$ and $\epsilon = \kappa \ell_c$ for the free membrane case [solid line, see Eq. (32)] and the confined membrane case [dashed line, see Eq. (35)], respectively. Here V is scaled by $S|\nabla c|/(128\pi \eta_m^2)$. The numbers in this plot indicate the slope of the curves and represent the powers of the algebraic dependencies.

in Appendix B that the asymptotic behaviors of V for $\delta \ll 1$ and $\delta \gg 1$ are

$$V^F \approx \frac{S|\nabla c|}{32\pi \eta_m^2} \ln \frac{L}{\ell_c} \quad (33)$$

and

$$V^F \approx \frac{13S|\nabla c|}{256\pi \eta_s^2} \frac{1}{\ell_c^2}, \quad (34)$$

respectively, where we choose $L \approx 1.85\nu^{-1}$. Note that Eq. (33) was previously derived in Ref. [19] for a 2D membrane, while Eq. (34) is a new result. As we see in Eqs. (33) and (34), there is a crossover from a logarithmic to an algebraic dependence with a power of -2 when δ is increased. These behaviors are consistent with the numerical plot in Fig. 4 for the free membrane case.

B. Confined membranes

Finally, we calculate the drift velocity for the confined membrane case. Substituting Eq. (13) into Eq. (3), we now obtain

$$V^C = - \frac{S|\nabla c|}{16\pi^2 \eta_m^2} \int_{\epsilon}^{\infty} d^2 w \Omega_{\beta\beta'\gamma\gamma'} \times \hat{n}_\alpha \frac{\partial^2 g_{\alpha\beta}^C(\mathbf{w})}{\partial w_\gamma \partial w_\delta} \frac{\partial g_{\delta\beta'}^C(\mathbf{w})}{\partial w_{\gamma'}} (\mathbf{w} \cdot \hat{\mathbf{n}}), \quad (35)$$

where $\epsilon = \kappa \ell_c$ and $g_{\alpha\beta}^C(\mathbf{w}) = 4\pi \eta_m G_{\alpha\beta}^C$ as before. In Fig. 4, we present numerically calculated V^C as a function of ϵ by the dashed line. As ϵ is increased, we see a crossover from a logarithmic to an algebraic dependence, although V^C decays faster than V^F at large scales.

TABLE I. Summary of the asymptotic dependencies of the thermal diffusion coefficient D_T , the active diffusion coefficient D_A , and the drift velocity V on the passive particle size ℓ_c . The numbers after the asymptotic expressions correspond to the equation numbers in this paper.

Cases	Limits	D_T	D_A	V
free membrane	$v\ell_c \ll 1$	$\ln(1/\ell_c)$ (26)	$\ln(1/\ell_c)$ (17)	$\ln(1/\ell_c)$ (33)
($hk \gg 1$)	$v\ell_c \gg 1$	$1/\ell_c$ (27)	$1/\ell_c^2$ (18)	$1/\ell_c^2$ (34)
confined membrane	$\kappa\ell_c \ll 1$	$\ln(1/\ell_c)$ (29)	$\ln(1/\ell_c)$ (22)	$\ln(1/\ell_c)$ (36)
($hk \ll 1$)	$\kappa\ell_c \gg 1$	$1/\ell_c^2$ (30)	$1/\ell_c^4$ (23)	$1/\ell_c^4$ (37)

The asymptotic behaviors of V^C for small and large ϵ values can be discussed similarly. Using Eqs. (20) and (21), we obtain in Appendix B the asymptotic expressions of V^C for $\epsilon \ll 1$ and $\epsilon \gg 1$ as

$$V^C \approx \frac{S|\nabla c|}{32\pi\eta_m^2} \ln \frac{L}{\ell_c} \quad (36)$$

and

$$V^C \approx \frac{3S|\nabla c|}{16\pi\eta_s^2} \frac{h^2}{\ell_c^4}, \quad (37)$$

respectively, and we choose $L \approx 3.05\kappa^{-1}$ to coincide with the numerical integration. We note that Eqs. (33) and (36) are identical and depend only on η_m for small sizes [19].

From Fig. 4 and Eqs. (33), (34), (36), and (37), we see that the drift velocity V is always positive. This means that passive particles move toward higher concentrations of active proteins, and a chemotaxis-like drift takes place in the presence of protein concentration gradients [19–21]. The dominant viscosity dependence of V switches from η_m to η_s as the particle size exceeds the corresponding hydrodynamic screening length, namely ν^{-1} or κ^{-1} .

VI. SUMMARY AND DISCUSSION

In this paper, we have investigated lateral diffusion induced by active force dipoles embedded in a biomembrane. In particular, we have calculated the active diffusion coefficient and the drift velocity for the free and the confined membrane cases by taking into account the hydrodynamic coupling between the membrane and the surrounding bulk solvent. The force dipole model in Refs. [19,20] and the general membrane mobility tensors obtained in Refs. [25–28] have been employed in our work. When the size of a passive diffusing particle is small, the active diffusion coefficients for the free and the confined membranes represent the same logarithmic size dependence, as shown in Eqs. (17) and (22), respectively [19]. In the opposite large size limit, we find algebraic dependencies with powers -2 and -4 for the two cases, as given by Eqs. (18) and (23), respectively. These are the important outcomes of this paper, and they are also summarized in Table I together with other asymptotic expressions.

In our work, we have assumed that the total diffusion coefficient is provided by the sum of thermal and nonthermal contributions. For small particle sizes, we have shown that both the total D^F and D^C exhibit a logarithmic size dependence [19], whereas different contributions have different size dependencies for large particle sizes. From this result, we have obtained

two characteristic length scales that describe the crossover from nonthermal to thermal behaviors when the particle size is larger than the hydrodynamic screening length. The drift velocity in the presence of a concentration gradient of active proteins exhibits the same size dependencies as the active diffusion coefficient for the two membrane geometries.

Here we give some numerical estimates of the obtained crossover length scales. Using typical values such as $k_B T \approx 4 \times 10^{-21}$ J, $\eta_s \approx 10^{-3}$ Pa s, $h \approx 10^{-9}$ m, $S \approx 10^{-42}$ J² s, and $c_0 \approx 10^{14}$ m⁻² [19], we obtain $\ell^* \approx 2 \times 10^{-6}$ m [see Eq. (28)] and $\ell^{**} \approx 6 \times 10^{-8}$ m [see Eq. (31)]. On the other hand, the SD and the ES screening lengths are typically $\nu^{-1} \approx 5 \times 10^{-7}$ m and $\kappa^{-1} \approx 2 \times 10^{-8}$ m, respectively [4,5,7,8]. Hence ℓ^* and ℓ^{**} are typically larger than ν^{-1} and κ^{-1} , respectively. Moreover, the values of S and c_0 can vary significantly in one membrane to another, as pointed out in Ref. [19]. For example, when active proteins are confined in raft domains [29–31], the 2D concentration c_0 can be much larger. When, for example, $c_0 \approx 10^{15}$ m⁻² (while S is the same as above) [21], the crossover length can be estimated as $\ell^* \approx 2 \times 10^{-5}$ m and $\ell^{**} \approx 2 \times 10^{-7}$ m. If ℓ^* and ℓ^{**} are much larger than the screening lengths ν^{-1} and κ^{-1} , respectively, as in this case, the three different scaling regimes of the total diffusion coefficient are expected as the particle size is increased, i.e., $\ln(1/\ell_c) \rightarrow 1/\ell_c^2 \rightarrow 1/\ell_c$ for the free membrane case, and $\ln(1/\ell_c) \rightarrow 1/\ell_c^4 \rightarrow 1/\ell_c^2$ for the confined membrane case.

Momentum in a membrane is conserved over distances smaller than the hydrodynamic screening length (either ν^{-1} or κ^{-1}), whereas it leaks to the surrounding fluid beyond that length scale [32–34]. Within a membrane, the velocity decays as $\ln(1/r)$ at short distances, as shown in Eqs. (15) and (20), due to the momentum conservation in two dimensions. These 2D behaviors also lead to the logarithmic dependence of the active diffusion coefficients in Eqs. (17) and (22). For the free membrane case, the velocity decays as $1/r$ at large scales as shown in Eq. (16) due to the momentum conservation in the 3D bulk. This behavior is reflected in the first term of Eq. (27) for the thermal diffusion coefficient [6]. As shown in Eq. (21), however, the velocity decays as $1/r^2$ at large scales for the confined membrane case. This behavior essentially arises from the mass conservation in two dimensions while the total momentum is not conserved due to the presence of the walls, which break the translational symmetry of the system [32–34]. The corresponding contribution is the first term of Eq. (30) for the thermal diffusion coefficient [7,8].

The active diffusion coefficient D_A^F obtained in Eq. (18) for the free membrane case essentially reflects the hydrodynamics of the surrounding bulk 3D solvent. Hence our result can be compared with that in Ref. [19] obtained for a purely 3D fluid

system:

$$D_A^{3D} \approx \frac{Sc_0^{3D}}{60\pi\eta_s^2} \frac{1}{\ell_c}, \quad (38)$$

which decays as $1/\ell_c$ and is different from Eq. (18). In fact, such a difference arises from the different dimensions of the dipole concentrations, i.e., c_0 is the 2D concentration in our case, while c_0^{3D} is the 3D concentration in Ref. [19]. A similar comparison can also be made for the drift velocity of free membranes in Eq. (34) and that in Ref. [19] for a 3D fluid system:

$$V^{3D} \approx \frac{S|\nabla c^{3D}|}{30\pi\eta_s^2} \frac{1}{\ell_c}. \quad (39)$$

The same reason holds for the different ℓ_c -dependence.

At this stage, we also comment that both the active diffusion coefficient D_A and the drift velocity V exhibit the same ℓ_c -dependence. Although the integrands in Eqs. (1) and (3) look apparently different, their physical dimensions are identical because the first derivative of the mobility tensor in Eq. (1) corresponds to the product of the second derivative and $(\mathbf{r} \cdot \hat{\mathbf{n}})$ in Eq. (3). This is the simple reason that they exhibit the same ℓ_c -dependence. One can also easily confirm that V is positive when we make use of the membrane mobility tensor, because the integrand in Eq. (3) is the product of the first and the second derivatives of the mobility tensor, which have opposite signs. This leads to $V > 0$ indicating a chemotaxis-like drift, as mentioned before.

In this work, we have assumed that active proteins generate forces only in the lateral directions. On the other hand, actual active motors such as bacteriorhodopsin can also exert forces to the surrounding solvent [16–18]. Although we did not take into account such normal forces that induce membrane undulation, consideration of normal forces as well as lateral ones will provide us with a general understanding of active diffusion in biomembranes [37].

We have also assumed that the force dipoles are fixed in a membrane and are distributed homogeneously. It would be interesting to consider the case when active proteins can also move laterally in the membrane and even interact with each other through a nematic-like interaction [38]. The full equation of motion now involves potential-of-mean-force interactions in the multiparticle diffusion equations that describe the combined motions of the passive particle and active proteins in the membrane. Although the dynamics of the active protein concentration is essentially determined by a diffusion equation, it is a complicated problem because not only thermal diffusion but also active nonthermal diffusion should be taken into account. Our work is a step toward such a full description of very rich biomembrane dynamics.

ACKNOWLEDGMENTS

We thank A. S. Mikhailov and T. Kato for useful discussions. S.K. and R.O. acknowledge support from a Grant-in-Aid for Scientific Research on Innovative Areas “*Fluctuation and Structure*” (Grant No. 25103010) from the Ministry of Education, Culture, Sports, Science, and Technology of Japan, and a Grant-in-Aid for Scientific Research (C) (Grant No. 15K05250) from the Japan Society for the Promotion of Science (JSPS).

APPENDIX A: DERIVATION OF EQS. (18) AND (23)

Since Eqs. (17) and (22) have been obtained in Ref. [19], we show here the derivation of Eqs. (18) and (23). Substituting Eq. (16) into Eq. (14), we get

$$D_A^F = \frac{Sc_0}{8\pi^2\eta_m^2} \int_{\delta}^{\infty} d^2z \Omega_{\beta\beta'\gamma\gamma'} \times \frac{\partial}{\partial z_{\gamma}} \left(\frac{\hat{z}_{\alpha}\hat{z}_{\beta}}{z} \right) \frac{\partial}{\partial z_{\gamma'}} \left(\frac{\hat{z}_{\alpha}\hat{z}_{\beta'}}{z} \right), \quad (A1)$$

where $\mathbf{z} = \nu\mathbf{r}$. Since

$$\frac{\partial}{\partial z_{\gamma}} \left(\frac{\hat{z}_{\alpha}\hat{z}_{\beta}}{z} \right) = \frac{1}{z^3} (\delta_{\alpha\gamma}z_{\beta} + \delta_{\beta\gamma}z_{\alpha}) - \frac{3}{z^5} z_{\alpha}z_{\beta}z_{\gamma}, \quad (A2)$$

the integrand in Eq. (A1) becomes

$$\begin{aligned} & \frac{\partial}{\partial z_{\gamma}} \left(\frac{\hat{z}_{\alpha}\hat{z}_{\beta}}{z} \right) \frac{\partial}{\partial z_{\gamma'}} \left(\frac{\hat{z}_{\alpha}\hat{z}_{\beta'}}{z} \right) \\ &= \frac{1}{z^4} \delta_{\beta\gamma} \delta_{\beta'\gamma'} + \frac{1}{z^6} [\delta_{\gamma\gamma'} z_{\beta} z_{\beta'} - 2(\delta_{\beta\gamma} z_{\beta'} z_{\gamma'} + \delta_{\beta'\gamma'} z_{\beta} z_{\gamma})] \\ &+ \frac{3}{z^8} z_{\beta} z_{\beta'} z_{\gamma} z_{\gamma'}. \end{aligned} \quad (A3)$$

By operating $\Omega_{\beta\beta'\gamma\gamma'}$, we have

$$\Omega_{\beta\beta'\gamma\gamma'} \frac{\partial}{\partial z_{\gamma}} \left(\frac{\hat{z}_{\alpha}\hat{z}_{\beta}}{z} \right) \frac{\partial}{\partial z_{\gamma'}} \left(\frac{\hat{z}_{\alpha}\hat{z}_{\beta'}}{z} \right) = \frac{5}{8z^4}. \quad (A4)$$

After the integration, we obtain Eq. (18).

Similarly, we substitute Eq. (21) into Eq. (19) and obtain

$$D_A^C = \frac{Sc_0}{8\pi^2\eta_m^2} \int_{\epsilon}^{\infty} d^2w \Omega_{\beta\beta'\gamma\gamma'} \times \frac{\partial}{\partial w_{\gamma}} \left(\frac{\delta_{\alpha\beta} - 2\hat{w}_{\alpha}\hat{w}_{\beta}}{w^2} \right) \frac{\partial}{\partial w_{\gamma'}} \left(\frac{\delta_{\alpha\beta'} - 2\hat{w}_{\alpha}\hat{w}_{\beta'}}{w^2} \right), \quad (A5)$$

where $\mathbf{w} = \kappa\mathbf{r}$. Since

$$\begin{aligned} & \frac{\partial}{\partial w_{\gamma}} \left(\frac{\delta_{\alpha\beta} - 2\hat{w}_{\alpha}\hat{w}_{\beta}}{w^2} \right) \\ &= -\frac{2}{w^4} (\delta_{\alpha\beta} w_{\gamma} + \delta_{\beta\gamma} w_{\alpha} + \delta_{\alpha\gamma} w_{\beta}) + \frac{8}{w^6} w_{\alpha} w_{\beta} w_{\gamma}, \end{aligned} \quad (A6)$$

we obtain

$$\begin{aligned} & \frac{\partial}{\partial w_{\gamma}} \left(\frac{\delta_{\alpha\beta} - 2\hat{w}_{\alpha}\hat{w}_{\beta}}{w^2} \right) \frac{\partial}{\partial w_{\gamma'}} \left(\frac{\delta_{\alpha\beta'} - 2\hat{w}_{\alpha}\hat{w}_{\beta'}}{w^2} \right) \\ &= \frac{4}{w^6} \delta_{\beta\gamma} \delta_{\beta'\gamma'} + \frac{4}{w^8} [\delta_{\beta\beta'} w_{\gamma} w_{\gamma'} + \delta_{\beta'\gamma} w_{\beta} w_{\gamma'} \\ &+ \delta_{\beta\gamma'} w_{\beta'} w_{\gamma} + \delta_{\gamma\gamma'} w_{\beta} w_{\beta'} - 2(\delta_{\beta\gamma} w_{\beta'} w_{\gamma'} \\ &+ \delta_{\beta'\gamma'} w_{\beta} w_{\gamma})]. \end{aligned} \quad (A7)$$

By operating $\Omega_{\beta\beta'\gamma\gamma'}$, we have

$$\begin{aligned} & \Omega_{\beta\beta'\gamma\gamma'} \frac{\partial}{\partial w_{\gamma}} \left(\frac{\delta_{\alpha\beta} - 2\hat{w}_{\alpha}\hat{w}_{\beta}}{w^2} \right) \frac{\partial}{\partial w_{\gamma'}} \left(\frac{\delta_{\alpha\beta'} - 2\hat{w}_{\alpha}\hat{w}_{\beta'}}{w^2} \right) \\ &= \frac{4}{w^6}. \end{aligned} \quad (A8)$$

After the integration, we obtain Eq. (23).

APPENDIX B: DERIVATION OF EQS. (34) AND (37)

In this appendix, we show the derivation of Eqs. (34) and (37). Substituting Eq. (16) into Eq. (32), we obtain

$$V^F = -\frac{S|\nabla c|}{4\pi^2\eta_m^2} \int_{\delta}^{\infty} d^2z \Omega_{\beta\beta'\gamma\gamma'} \hat{n}_{\alpha} \frac{\partial^2}{\partial z_{\gamma} \partial z_{\delta}} \left(\frac{\hat{z}_{\alpha} \hat{z}_{\beta}}{z} \right) \frac{\partial}{\partial z_{\gamma'}} \left(\frac{\hat{z}_{\delta} \hat{z}_{\beta'}}{z} \right) (\mathbf{z} \cdot \hat{\mathbf{n}}). \quad (\text{B1})$$

In the above, the derivatives are

$$\frac{\partial^2}{\partial z_{\gamma} \partial z_{\delta}} \left(\frac{\hat{z}_{\alpha} \hat{z}_{\beta}}{z} \right) = \frac{1}{z^3} (\delta_{\alpha\delta} \delta_{\beta\gamma} + \delta_{\alpha\gamma} \delta_{\beta\delta}) - \frac{3}{z^5} (\delta_{\alpha\delta} z_{\beta} z_{\gamma} + \delta_{\beta\delta} z_{\alpha} z_{\gamma} + \delta_{\alpha\gamma} z_{\beta} z_{\delta} + \delta_{\beta\gamma} z_{\alpha} z_{\delta} + \delta_{\gamma\delta} z_{\alpha} z_{\beta}) + \frac{15}{z^7} z_{\alpha} z_{\beta} z_{\gamma} z_{\delta} \quad (\text{B2})$$

and

$$\begin{aligned} \frac{\partial^2}{\partial z_{\gamma} \partial z_{\delta}} \left(\frac{\hat{z}_{\alpha} \hat{z}_{\beta}}{z} \right) \frac{\partial}{\partial z_{\gamma'}} \left(\frac{\hat{z}_{\delta} \hat{z}_{\beta'}}{z} \right) = & -\frac{1}{z^6} [2\delta_{\beta'\gamma'} (\delta_{\alpha\gamma} z_{\beta} + \delta_{\beta\gamma} z_{\alpha}) - (\delta_{\alpha\gamma'} \delta_{\beta\gamma} + \delta_{\alpha\gamma} \delta_{\beta\gamma'}) z_{\beta'}] \\ & -\frac{3}{z^8} [(\delta_{\alpha\gamma'} z_{\beta} z_{\gamma} + \delta_{\beta\gamma'} z_{\alpha} z_{\gamma} - \delta_{\alpha\gamma} z_{\beta} z_{\gamma'} - \delta_{\beta\gamma} z_{\alpha} z_{\gamma'} + \delta_{\gamma\gamma'} z_{\alpha} z_{\beta}) z_{\beta'} - 2\delta_{\beta'\gamma'} z_{\alpha} z_{\beta} z_{\gamma}] \\ & -\frac{3}{z^{10}} z_{\alpha} z_{\beta} z_{\beta'} z_{\gamma} z_{\gamma'}. \end{aligned} \quad (\text{B3})$$

By operating $\Omega_{\beta\beta'\gamma\gamma'}$, we have

$$\Omega_{\beta\beta'\gamma\gamma'} \frac{\partial^2}{\partial z_{\gamma} \partial z_{\delta}} \left(\frac{\hat{z}_{\alpha} \hat{z}_{\beta}}{z} \right) \frac{\partial}{\partial z_{\gamma'}} \left(\frac{\hat{z}_{\delta} \hat{z}_{\beta'}}{z} \right) = -\frac{13z_{\alpha}}{8z^6}. \quad (\text{B4})$$

After the integration, we obtain Eq. (34).

Next we substitute Eq. (21) into Eq. (35) and find

$$V^C = -\frac{S|\nabla c|}{4\pi^2\eta_m^2} \int_{\epsilon}^{\infty} d^2w \Omega_{\beta\beta'\gamma\gamma'} \hat{n}_{\alpha} \frac{\partial^2}{\partial w_{\gamma} \partial w_{\delta}} \left(\frac{\delta_{\alpha\beta} - 2\hat{w}_{\alpha} \hat{w}_{\beta}}{w^2} \right) \frac{\partial}{\partial w_{\gamma'}} \left(\frac{\delta_{\delta\beta'} - 2\hat{w}_{\delta} \hat{w}_{\beta'}}{w^2} \right) (\mathbf{w} \cdot \hat{\mathbf{n}}). \quad (\text{B5})$$

Here the derivatives are

$$\begin{aligned} \frac{\partial^2}{\partial w_{\gamma} \partial w_{\delta}} \left(\frac{\delta_{\alpha\beta} - 2\hat{w}_{\alpha} \hat{w}_{\beta}}{w^2} \right) = & -\frac{2}{w^4} (\delta_{\alpha\beta} \delta_{\gamma\delta} + \delta_{\alpha\gamma} \delta_{\beta\delta} + \delta_{\alpha\delta} \delta_{\beta\gamma}) + \frac{8}{w^6} (\delta_{\alpha\beta} w_{\gamma} w_{\delta} + \delta_{\beta\delta} w_{\alpha} w_{\gamma} + \delta_{\alpha\delta} w_{\beta} w_{\gamma} \\ & + \delta_{\alpha\gamma} w_{\beta} w_{\delta} + \delta_{\beta\gamma} w_{\alpha} w_{\delta} + \delta_{\gamma\delta} w_{\alpha} w_{\beta}) - \frac{48}{w^8} w_{\alpha} w_{\beta} w_{\gamma} w_{\delta} \end{aligned} \quad (\text{B6})$$

and

$$\begin{aligned} \frac{\partial^2}{\partial w_{\gamma} \partial w_{\delta}} \left(\frac{\delta_{\alpha\beta} - 2\hat{w}_{\alpha} \hat{w}_{\beta}}{w^2} \right) \frac{\partial}{\partial w_{\gamma'}} \left(\frac{\delta_{\delta\beta'} - 2\hat{w}_{\delta} \hat{w}_{\beta'}}{w^2} \right) = & -\frac{4}{w^8} [3\delta_{\beta'\gamma'} (\delta_{\alpha\beta} w_{\gamma} + \delta_{\alpha\gamma} w_{\beta} + \delta_{\beta\gamma} w_{\alpha}) \\ & - (\delta_{\alpha\beta} \delta_{\gamma\beta'} + \delta_{\alpha\gamma} \delta_{\beta\beta'} + \delta_{\alpha\beta'} \delta_{\beta\gamma}) w_{\gamma'} - (\delta_{\alpha\beta} \delta_{\gamma\gamma'} + \delta_{\alpha\gamma} \delta_{\beta\beta'} + \delta_{\alpha\gamma'} \delta_{\beta\beta'}) w_{\beta'}] \\ & + \frac{16}{w^{10}} [(\delta_{\alpha\beta} w_{\beta'} w_{\gamma} - \delta_{\beta\beta'} w_{\alpha} w_{\gamma} - \delta_{\alpha\beta'} w_{\beta} w_{\gamma} \\ & + \delta_{\alpha\gamma} w_{\beta} w_{\beta'} + \delta_{\beta\gamma} w_{\alpha} w_{\beta'} - \delta_{\beta'\gamma} w_{\alpha} w_{\beta}) w_{\gamma'} \\ & - (\delta_{\beta'\gamma'} w_{\alpha} w_{\gamma} + \delta_{\alpha\gamma'} w_{\beta} w_{\gamma} + \delta_{\gamma\gamma'} w_{\alpha} w_{\beta}) w_{\beta'} + 3\delta_{\beta'\gamma'} w_{\alpha} w_{\beta} w_{\gamma}]. \end{aligned} \quad (\text{B7})$$

By operating $\Omega_{\beta\beta'\gamma\gamma'}$, we find

$$\Omega_{\beta\beta'\gamma\gamma'} \frac{\partial^2}{\partial w_{\gamma} \partial w_{\delta}} \left(\frac{\delta_{\alpha\beta} - 2\hat{w}_{\alpha} \hat{w}_{\beta}}{w^2} \right) \frac{\partial}{\partial w_{\gamma'}} \left(\frac{\delta_{\delta\beta'} - 2\hat{w}_{\delta} \hat{w}_{\beta'}}{w^2} \right) = -\frac{12w_{\alpha}}{w^8}. \quad (\text{B8})$$

After the integration, we obtain Eq. (37).

- [1] S. J. Singer and G. L. Nicolson, *Science* **175**, 720 (1972).
 [2] B. Alberts, A. Johnson, P. Walter, J. Lewis, and M. Raff, *Molecular Biology of the Cell* (Garland Science, New York, 2008).
 [3] R. Lipowsky and E. Sackmann, *Structure and Dynamics of Membranes* (Elsevier, Amsterdam, 1995).

- [4] P. G. Saffman and M. Delbrück, *Proc. Natl. Acad. Sci. (USA)* **72**, 3111 (1975).
 [5] P. G. Saffman, *J. Fluid Mech.* **73**, 593 (1976).
 [6] B. D. Hughes, B. A. Pailthorpe, and L. R. White, *J. Fluid Mech.* **110**, 349 (1981).
 [7] E. Evans and E. Sackmann, *J. Fluid Mech.* **194**, 553 (1988).

- [8] S. Ramachandran, S. Komura, M. Imai, and K. Seki, *Eur. Phys. J. E* **31**, 303 (2010).
- [9] K. Seki, S. Ramachandran, and S. Komura, *Phys. Rev. E* **84**, 021905 (2011).
- [10] K. Seki, S. Mogre, and S. Komura, *Phys. Rev. E* **89**, 022713 (2014).
- [11] S. Komura, S. Ramachandran, and M. Imai, in *Non-Equilibrium Soft Matter Physics*, edited by S. Komura and T. Ohta (World Scientific, Singapore, 2012), p. 197.
- [12] B. R. Parry, I. V. Surovtsev, M. T. Cabeen, C. S. O'Hern, E. R. Dufresne, and C. Jacobs-Wagner, *Cell* **156**, 183 (2014).
- [13] M. Guo, A. J. Ehrlicher, M. H. Jensen, M. Renz, J. R. Moore, R. D. Goldman, J. Lippincott-Schwartz, F. C. Mackintosh, and D. A. Weitz, *Cell* **158**, 822 (2014).
- [14] K. Yasuda, R. Okamoto, S. Komura, and A. S. Mikhailov, *Europhys. Lett.* **117**, 38001 (2017).
- [15] K. Yasuda, R. Okamoto, and S. Komura, *Phys. Rev. E* **95**, 032417 (2017).
- [16] J.-B. Manneville, P. Bassereau, D. Lévy, and J. Prost, *Phys. Rev. Lett.* **82**, 4356 (1999).
- [17] J.-B. Manneville, P. Bassereau, S. Ramaswamy, and J. Prost, *Phys. Rev. E* **64**, 021908 (2001).
- [18] S. Ramaswamy, J. Toner, and J. Prost, *Phys. Rev. Lett.* **84**, 3494 (2000).
- [19] A. S. Mikhailov and R. Kapral, *Proc. Natl. Acad. Sci. (USA)* **112**, E3639 (2015).
- [20] R. Kapral and A. S. Mikhailov, *Physica D* **318**, 100 (2016).
- [21] Y. Koyano, H. Kitahata, and A. S. Mikhailov, *Phys. Rev. E* **94**, 022416 (2016).
- [22] M.-J. Huang, A. S. Mikhailov, and H.-Y. Chen, *Eur. Phys. J. E* **35**, 119 (2012).
- [23] M.-J. Huang, R. Kapral, A. S. Mikhailov, and H.-Y. Chen, *J. Chem. Phys.* **138**, 195101 (2013).
- [24] M. Tanaka and E. Sackmann, *Nature (London)* **437**, 656 (2005).
- [25] K. Inaura and Y. Fujitani, *J. Phys. Soc. Jpn.* **77**, 114603 (2008).
- [26] S. Ramachandran, S. Komura, K. Seki, and G. Gompper, *Eur. Phys. J. E* **34**, 46 (2011).
- [27] S. Ramachandran, S. Komura, K. Seki, and M. Imai, *Soft Matter* **7**, 1524 (2011).
- [28] S. Komura, S. Ramachandran, K. Seki, and M. Imai, *Adv. Planar Lipid Bilayers Liposomes* **16**, 129 (2012).
- [29] K. Simons and E. Ikonen, *Nature (London)* **387**, 569 (1997).
- [30] S. Komura and D. Andelman, *Adv. Colloid Interface Sci.* **208**, 34 (2014).
- [31] D. Lingwood and K. Simons, *Science* **327**, 46 (2010).
- [32] H. Diamant, *J. Phys. Soc. Jpn.* **78**, 041002 (2009).
- [33] N. Oppenheimer and H. Diamant, *Biophys. J.* **96**, 3041 (2009).
- [34] N. Oppenheimer and H. Diamant, *Phys. Rev. E* **82**, 041912 (2010).
- [35] E. P. Petrov and P. Schwille, *Biophys. J.* **94**, L41 (2008).
- [36] E. P. Petrov and P. Schwille, *Soft Matter* **8**, 7552 (2012).
- [37] S. Komura, K. Yasuda, and R. Okamoto, *J. Phys.: Condens. Matter* **27**, 432001 (2015).
- [38] A. W. C. Lau and T. C. Lubensky, *Phys. Rev. E* **80**, 011917 (2009).